

Hot Paper

The Role of Crystalline Intermediates in Mechanochemical Cyclorhodation Reactions Elucidated by in-Situ X-ray Powder Diffraction and Computation

José G. Hernández,^{*[a]} Karen J. Ardila-Fierro,^[a] Sara Gómez,^[b] Tomislav Stolar,^[c] Mirta Rubčić,^[d] Edi Topić,^[d] Cacier Z. Hadad,^[e] and Albeiro Restrepo^[e]

The occurrence of crystalline intermediates in mechanochemical reactions might be more widespread than previously assumed. For example, a recent study involving the acetate-assisted C–H activation of N–Heterocycles with [Cp*RhCl₂]₂ by ball milling revealed the formation of transient cocrystals between the reagents prior to the C–H activation step. However, such crystalline intermediates were only observed through stepwise intervallic ex-situ analysis, and their exact role in the C–H activation process remained unclear. In this study, we monitored the formation of discrete, stoichiometric cocrystals between benzo[h]quinoline and [Cp*RhCl₂]₂ by ball milling using in-situ synchrotron X-ray powder diffraction. This continuous analysis revealed an initial cocrystal that transformed into

a second crystalline form. Computational studies showed that differences in noncovalent interactions made the [Cp*RhCl₂]₂ unit in the later-appearing cocrystal more reactive towards NaOAc. This demonstrated the advantage of cocrystal formation before the acetate-assisted metalation–deprotonation step, and how the net cooperative action of weak interactions between the reagents in mechanochemical experiments can lead to stable supramolecular assemblies, which can enhance substrate activation under ball-milling conditions. This could explain the superiority of some mechanochemical reactions, such as acetate-assisted C–H activation, compared to their solution-based counterparts.

Introduction

The use of mechanochemical techniques (e.g., ball milling, twin-screw extrusion, acoustic magnetic resonance, etc.) for chemical synthesis has enabled the development of known and new transformations more sustainably.^[1,2] Particularly interesting are the examples in which mechanochemistry has shown the ability to alter reaction mechanisms or to change product

composition of well-established reactions.^[3–5] There are various explanations as to why a reaction may proceed more effectively through mechanochemistry compared to in solution, as well as reasons for the eventual switch in reactivity by mechanochemistry.^[3–5]

For instance, mechanochemical reactions by ball milling are almost always carried out under neat conditions or using only small amounts of solvents.^[6,7] In the absence of bulk solvents highly concentrated reaction conditions are created that affect the mobility of the reactants and influence reaction kinetics, thus sometimes facilitating the formation or isolation of metastable products.^[8,9] Complementarily, in the cases when a small amount of a liquid phase is used during the milling experiment, the chosen solvent is typically not sufficient or compatible to dissolve the reactants or products, therefore minimizing the solvation effects. In both cases, mechanochemical conditions can foster the advent of noncovalent interactions among the reactants,^[10] which in solution would be weaker or absent. Such conditions can lead to the isolation of labile products that would remain otherwise elusive.^[11–13]

In this context, a recent study by Koby et al. reported the successful mechanosynthesis and characterization of a tetrakis(trimethylsilylallyl)tin(IV) complex in solid state.^[14] Remarkably, the isolation of this product from solution proved difficult as the presence of solvents disrupts the noncovalent forces responsible for the stabilization of the molecular structure in the metal complex.^[14] Consequently, providing the conditions for noncovalent interactions to arise and guide chemical transformations could be another advantageous aspect of mechanochemical methods. Often, this feature is only

[a] Prof. Dr. J. G. Hernández, Dr. K. J. Ardila-Fierro
Grupo Ciencia de los Materiales, Instituto de Química
Facultad de Ciencias Exactas y Naturales, Universidad de Antioquia
Calle 70 No 52–21, Medellín (Colombia)
E-mail: joseg.hernandez@udea.edu.co
Homepage: <http://www.udea.edu.co/wps/portal/udea/web/inicio/investigacion/grupos-investigacion/ciencias-naturales-exactas/ciencia-materiales>

[b] Dr. S. Gómez
Scuola Normale Superiore, Classe di Scienze
Piazza dei Cavalieri 7, 56126 Pisa, (Italy)

[c] Dr. T. Stolar
Division of Physical Chemistry, Ruđer Bošković Institute
Bijenička c. 54, 10000 Zagreb (Croatia)

[d] Prof. Dr. M. Rubčić, Dr. E. Topić
Faculty of Science Department of Chemistry
University of Zagreb
Horvatovac 102a, 10000 Zagreb (Croatia)

[e] Prof. Dr. C. Z. Hadad, Prof. Dr. A. Restrepo
Instituto de Química
Facultad de Ciencias Exactas y Naturales Universidad de Antioquia, UdeA
Calle 70 No 52–21, Medellín (Colombia)

Supporting information for this article is available on the WWW under <https://doi.org/10.1002/chem.202301290>

speculated based on the outcome of a mechanochemical reaction, but in 2018 Lukin et al. clearly demonstrated the existence of a cocrystal intermediate between the organic reactants in a mechanochemical Knoevenagel reaction.^[15a] Even though the formation of crystalline intermediates is common in mechanochemical synthesis of metal–organic materials^[16,17] (e.g., MOFs, ZIFs, etc.), processes of covalent bond formation governed or templated by noncovalent forces are scarce,^[15a–b] with examples including topochemical reactions using cocrystallization to induce photodimerization under mechanochemical and photochemical conditions.^[18]

In the Knoevenagel reaction, the transient cocrystal was detected by in-situ Raman spectroscopy monitoring and its structural characterization revealed weak intermolecular N–H···O hydrogen bonding, which oriented the reactive centers for the condensation reaction to occur.^[15] Recently, we reported another example of cocrystal intermediates in mechanochemical reactions, this time during the formation of a metal–carbon bond.^[19] Specifically, while ex-situ monitoring the mechanochemical acetate-assisted C–H activation of pyridine and quinoline derivatives with $[\text{Cp}^*\text{MCl}_2]_2$ (M=Rh, Ir), we observed the presence of crystalline intermediates between the heterocyclic substrates and the metal complexes prior to the C–H activation step (Scheme 1a).^[19] Structural analysis of the cocrystals revealed that noncovalent interactions, favored under the solventless mechanochemical reaction conditions, played an important role in the stabilization of the crystalline phases. Interestingly, the formation of cocrystal intermediates in the mechanochemical protocol seems to correspond to an alteration to the generally accepted mechanism for the acetate-assisted C–H activation,^[20–23] which in solution begins with the rupture of the chloride-bridged rhodium dimer **1** by acetate ions before the involvement of the substrate in the C–H activation step (Scheme 1b).

Intrigued by the apparent mechanistic differences in acetate-assisted cyclorhodations by ball milling,^[19] and the reported superiority of mechanochemistry to synthesize rhodacyclic complexes,^[24] in the present work we study the formation of crystalline intermediates in the reaction of benzo[*h*]quinoline (BHQ; **2**) with $[\text{Cp}^*\text{RhCl}_2]_2$ (**1**, $\text{Cp}^* = \eta^5\text{-C}_5\text{Me}_5$), this time by in-situ

monitoring using synchrotron X-ray powder diffraction. Such a real-time and continuous examination of the reaction enabled us to unequivocally demonstrate the formation of two cocrystals, **4 α** and **4 β** , during the milling process and not as an artifact of the ex-situ analysis. Additionally, experimental and computational investigations enabled us to pinpoint the origin of the stability in **4 α** and **4 β** (Scheme 1a) as well as revealing their structural and electronic differences. For example, disparities in the crystal packing between both cocrystals and differences in their intermolecular interactions make the $[\text{Cp}^*\text{RhCl}_2]_2$ units in **4 β** more activated towards the reaction with NaOAc than in cocrystal **4 α** . Thus, proving the beneficial intermediacy of **4 β** in the mechanochemical C–H bond cleavage of BHQ with $[\text{Cp}^*\text{RhCl}_2]_2$ and NaOAc.

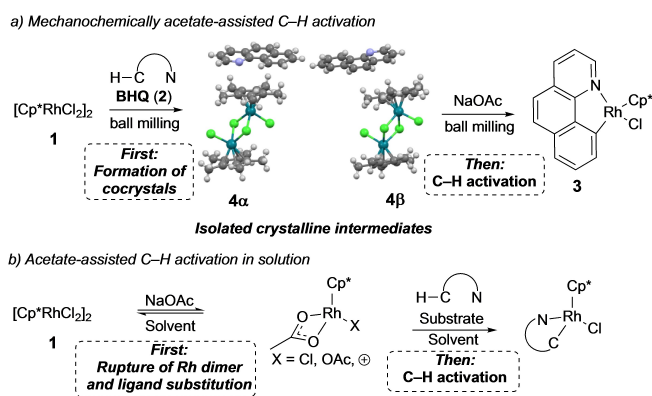
Results and Discussion

In-situ synchrotron X-ray powder diffraction monitoring

The presence of cocrystals during the mechanochemical acetate-assisted cyclometallations was originally observed by ex-situ analysis wherein the milling is repeatedly stopped and the milling jar is opened to sample the reaction mixture.^[19] Although informative, step-by-step ex-situ analysis can strongly affect the reaction course due to the multiple interruptions, which expose the reaction mixture to air, humidity and allow it to thermally and mechanically relax while sampling.^[25,26] Aware of this, we decided to monitor the milling process of $[\text{Cp}^*\text{RhCl}_2]_2$ (**1**) with benzo[*h*]quinoline (**2**) in situ by synchrotron powder X-ray diffraction (Figure 1). Since its introduction,^[27] this approach has been used to follow in real-time mechanochemical milling reactions permitting the observation of multistep transformations, reaction kinetics, and the discovery of new materials.^[25–30] However, in-situ monitoring of mechanochemical reactions such as metal-mediated C–H activations has only been developed by Raman spectroscopy,^[31–34] while real-time monitoring by synchrotron powder X-ray diffraction remains unexplored. Thus, to deepen our understanding in this area we began this study.

In an initial experiment $[\text{Cp}^*\text{RhCl}_2]_2$ (**1**; 0.24 mmol), BHQ (**2**) (0.48 mmol; 2.0 equiv.), and one ZrO_2 ball (weighing 3.4 g) were charged inside a poly(methyl)methacrylate (PMMA) milling jar under an atmosphere of air. Subsequently, this solid mixture was milled at 30 Hz in a mixer mill. PXRD monitoring of the reaction was performed by synchrotron X-ray diffraction ($\lambda = 0.20741 \text{ \AA}$ (for details, see the Supporting Information). After only 3 min of milling a new set of diffraction signals belonging to cocrystal **4 α** were observed (Figure 1). Importantly, just as in our previous report^[19] another crystalline phase with a major peak at 1.7° was observed early during the milling process but its structure could not be identified. Upon further milling, the intensity of the diffraction patterns for **4 α** increased and after 18 min the presence of a second cocrystal, namely **4 β** was detected (Figure 1).

Both cocrystals **4 α** and **4 β** coexisted for about 20 min but after 40 min of milling only the latter persisted, and it remained



Scheme 1. Acetate-assisted C–H activation by mechanochemistry and in solution.

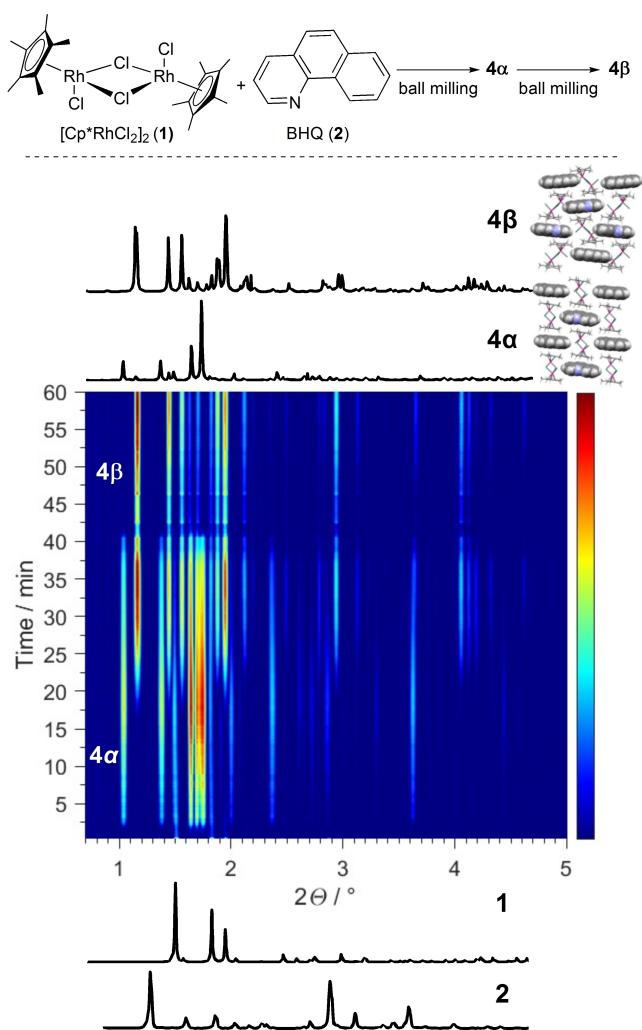


Figure 1. Time-resolved diffractograms for the reaction of $[\text{Cp}^*\text{RhCl}_2]_2$ (**1**; 0.24 mmol), BHQ (2.0 equiv.) at 30 Hz ($\lambda = 0.20741 \text{ \AA}$). PXRD patterns of **4α**, **4β**, **1**, and **2** are given on the top and at the bottom of the 2D plot. Crystallographic data used in the PXRD analysis: **1** (CLCPRH), **4α** (XAWPUK), and **4β** (XAWPUK01).

unchanged up to 1 h of milling. During the in-situ monitoring other transient crystalline phases (e.g., see peaks at 3.3° and 4.5°) were observable but their identification was not possible, only cocrystals **4α** and **4β** were characterized by single-crystal X-ray diffraction. Structurally, **4α** and **4β** are 1:2 cocrystals in which C–H...Cl and C–H... π interactions stabilize the corresponding supramolecular assemblies, the latter being more predominant in **4α**. The major difference between the two $[\text{Cp}^*\text{RhCl}_2]_2$ fragments in **4α** and **4β** is the relative orientation of the Cp* rings (Figure 2). Stacking interactions such as the ones identified in **4α** and **4β** have been found in cyclopentadienyl (Cp) complexes due to oppositely charged regions of electrostatic potential.^[35] Moreover, similar noncovalent interactions were recognized as dominant and responsible for the arrangement in the crystal structures of solid-state complexes of sex hormones with arenes made by mechanochemistry.^[36,37]

Differential scanning calorimetry and in-situ variable-temperature powder X-ray diffraction analysis

To evaluate the thermal stability of the cocrystals and to investigate the polymorphic transformation of **4α** into **4β** we used differential scanning calorimetry (DSC) and in-situ variable-temperature powder X-ray diffraction (VT-PXRD; Figure 3).

DSC measurements of **4α** and **4β** carried out from room temperature (25°C) to 300°C evidenced similar energetic profiles for both cocrystals with an initial endothermic event at 48°C (Figure 3a), which is close to the melting point ($48\text{--}50^\circ\text{C}$) of BHQ (**2**; see Figures S4 and S9 in the Supporting Information). The presence of BHQ (**2**) in the final mixture was expected since we milled **1** and **2** in a 1:2 stoichiometric ratio and cocrystals **4α** and **4β** contain **1** and **2** in a 1:1 ratio in their asymmetric units. The reason to use 2 equivalents of BHQ (**2**) was justified as the eventual cyclorhodation reaction requires a 1:2 stoichiometric ratio between **1** and **2**. But formation of the cocrystals can also be achieved by milling **1** and **2** in a 1:1 stoichiometric

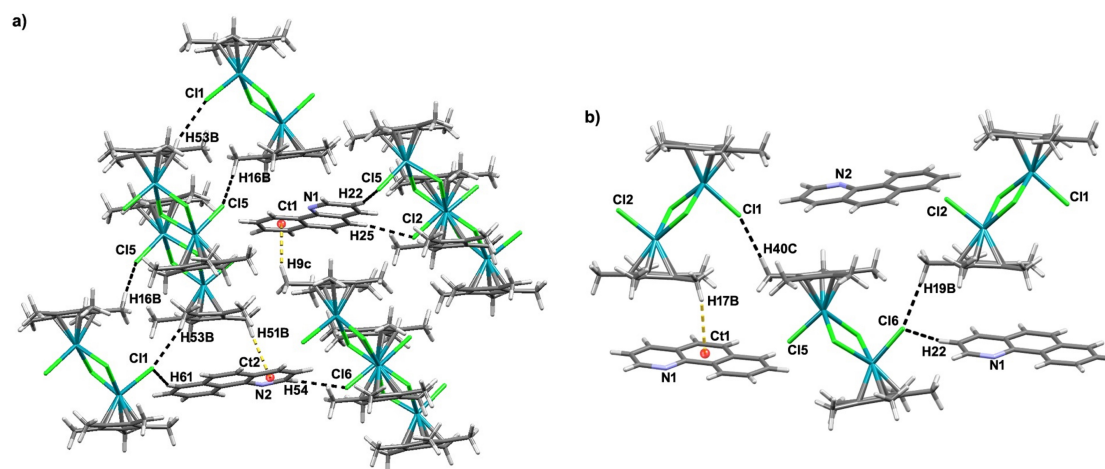


Figure 2. Crystal packing in a) **4α** and b) **4β**. C–H...Cl interactions are highlighted as black dashed lines; C–H... π interactions are highlighted in yellow. In (a), Ct1 and Ct2 refers to the centroids of the outer aromatic rings of BHQ molecules, while in (b) Ct1 refers to the centroid of the inner aromatic ring of BHQ.

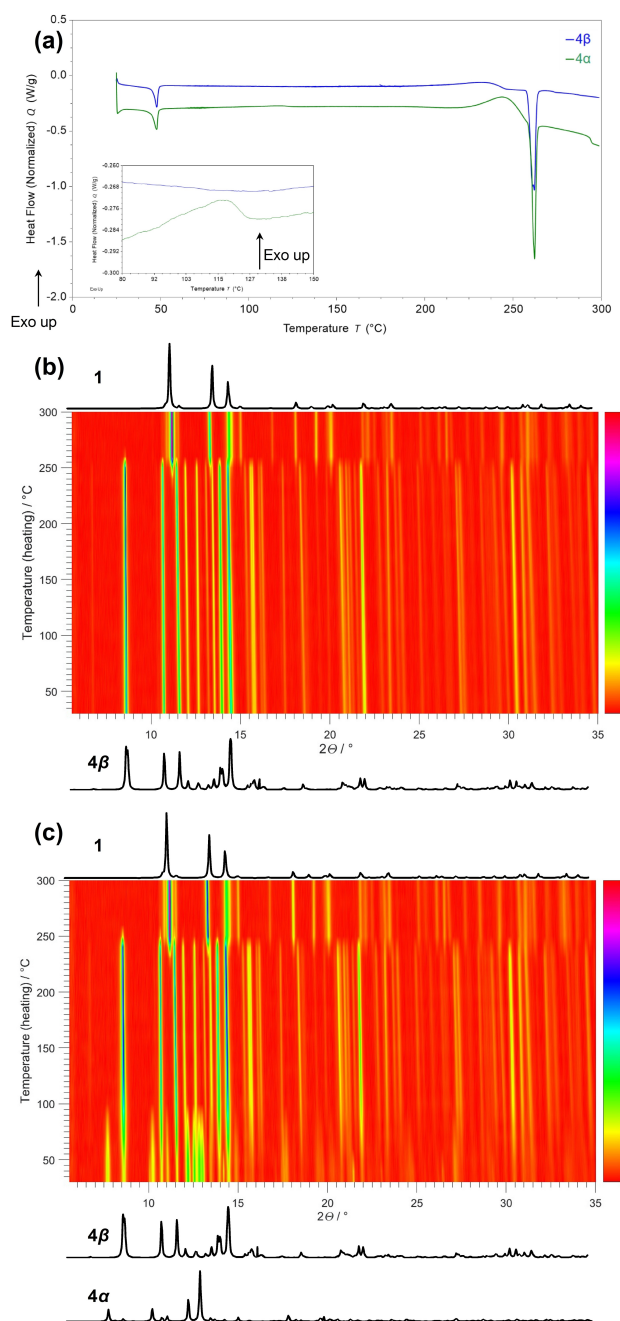


Figure 3. a) DSC traces of **4α** and **4β**. The inset shows a detail at 120 °C. b) In-situ variable temperature powder X-ray diffraction (VT-PXRD) patterns for cocystal **4β** ($\lambda = 1.54 \text{ \AA}$) and c) VT-PXRD patterns for a mixture initially containing **4α** and **4β** ($\lambda = 1.54 \text{ \AA}$).

ratio. In this case, the DSC analysis showed no residual BHQ (**2**) (Figure S12).

Importantly, in the case of **4α** the DSC analysis showed a change around 120 °C, which could be assigned to the polymorphic transition of **4α** to **4β**, even though the observed heat flow change is small (Figure 3a, inset), while a second endothermic peak for **4α** and **4β** was observed at 262 °C, which can be assigned to the evaporation of BHQ as the decomposition of **1** occurs at > 300 °C (Figure S8). In between these events, a broad exothermic peak could be tentatively related to

dissolution of **4β** in liquid BHQ, and/or strain relief in the solid **4β** particles (Figure 3a and S7).

Based on the information from the DSC experiment, samples of **4α** and **4β** were analyzed by VT-PXRD from 30 to 300 °C with 10 °C steps. In the case of **4β** its PXRD pattern remained unchanged until 240 °C when a new set of diffraction peaks began appearing (Figure 3b), which belong to $[\text{Cp}^*\text{RhCl}_2]_2$ (**1**). The new diffraction pattern became predominant at 260 °C and persisted up to 300 °C. This process evidenced the loss of BHQ due to evaporation and the disassembling of **4β**. In a second experiment a sample containing **4α** and **4β** was also analyzed by VT-PXRD (Figure 3c). In this case, at 50 °C the diffraction peaks corresponding to **4α** became attenuated whereas the characteristic diffraction features of **4β** gained intensity evidencing a thermally promoted phase transition.

Knowing that under ball milling conditions the temperature of the milling assembly does not exceed 30 °C, as confirmed in a previous study,^[38] the polymorphic transformation of **4α** to **4β** by ball milling can be regarded as mostly mechanically driven (Figure 1). This is confirmed by the harsher conditions required by heating (ca. 100 °C) to reach full conversion of cocystal **4α** into **4β** (Figure 3c). These observations are in line with a recent study on the polymorphism in stoichiometric organic cocrystals in which solid-state transformations by ball milling were promoted at temperatures lower than those required by heating alone.^[39] Finally, as showed in Figure 3c, once **4β** was formed from **4α** its behavior in the VT-PXRD experiment was identical to the pristine cocystal **4β** (Figure 3b–c).

Computational studies

To investigate the origin of the relative stabilities in **4α** and **4β** we employed two computational strategies. On the one hand we calculated interaction energies, bonding descriptors, and reactivity indices in the solid using periodic boundary conditions on a replicating unit cell and repeated the same calculations on clusters of growing size within the unit cell. Interaction energies were calculated as $E_{\text{interaction}} = E_{\text{complex}} - E_{\text{fragments}}$ for the clusters. In the extended solids we used periodic energy decomposition analysis (PEDA), and interaction energies were calculated with respect to the fragments, defining two regions, one containing the BHQ (**2**) fragments and the other containing the bare rhodium complex (Rc; **1**).^[40a] On the other, the clusters were grown vertically by sequentially adding BHQ units to the Rc in the following stoichiometries: Rc + BHQ, Rc + 2BHQ, 2Rc + 2BHQ, 2Rc + 3BHQ (Figure 4a).

Experimental geometries derived from crystallographic data have some degree of uncertainty so that they must undergo further optimization to reproduce cell parameters and other properties, accordingly, in order to account for the effect of polarization in the basis set and for dispersion in our calculations, we estimated differences in binding energies between the α and β forms following this rigorous progression in the extended solids (see Table S1 for the corresponding results): First, we calculated single point energies on the solid

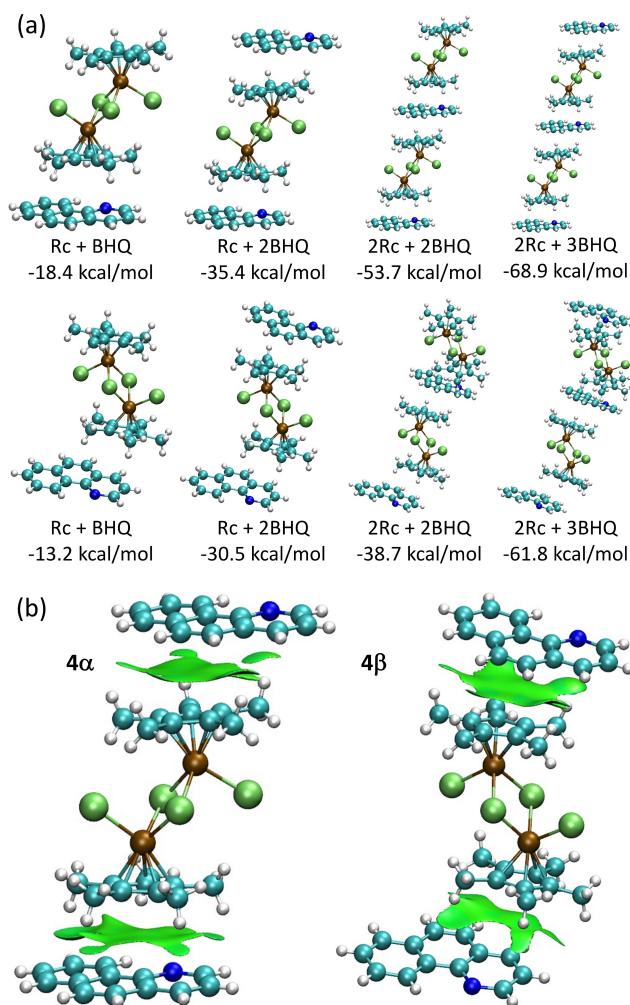


Figure 4. a) Geometries of layers of **4α** (top) and **4β** (bottom) with indication of the binding energy (Rc = [Cp*RhCl₂]₂; BHQ = benzo[*h*]quinoline) at the PBE–D3/DZP level of theory. b) Noncovalent interaction surfaces for the cocrystals **4α** and **4β**.

geometries using the PBE/DZ, PBE-D3/DZ and PBE-D3/DZP model chemistries^[41a–c] and obtained a 9.3 kcal·mol^{−1} in favor of **α** with the latter. Second, we optimized the crystal geometries and cell parameters with periodic boundary conditions under DFTB at the (GFN1-xTB)^[40b] level with D3-BJ dispersion corrections and repeated the PBE-D3/DZP single point energy calculations on those geometries, this yielded 9.4 kcal·mol^{−1} in favor of **α**. Third, we optimized both crystals at the PBE-D3/DZP level and obtained 6.4 kcal·mol^{−1} in favor of **α**. For the model clusters, only PBE/DZ, PBE-D3/DZ and PBE-D3/DZP single point energy calculations on the experimental geometries were carried out; the corresponding results are listed in Table S2.

Variation of the cell parameters during the optimization and the differences between the experimental and optimized geometries are provided in Table S3 and Figures S14–S17. In what follows, we base our discussion in the results obtained with the best method, namely, PBE-D3/DZP. We used the following programs: AMS,^[42] AMS-BAND,^[43,44] AMS-QTAIM,^[45] NCI,^[46a] and NCIPLLOT.^[46b]

On the basis of purely electronic energies (not normalized by the number of units), Figure 4a shows that **4α** is favored over **4β** in every single cluster stoichiometry by 5.2, 4.9, 15.0, 7.1 kcal·mol^{−1}. The 7.1 kcal·mol^{−1} difference for the cluster that more closely resembles the solid (2Rc + 3BHQ) is consistent with the extended solid calculations which afford a difference of 6.4 kcal·mol^{−1} in favor of **4α**. Accounting for the basis set superposition error (BSSE) using the Counterpoise correction of Boys and Bernardi^[47a] slightly reduces the energy difference between the clusters to 3.0, 2.9, 10.9, 3.2 kcal·mol^{−1} respectively, always in favor of the **α** form. Notice that in purely organic crystals, difference in energies among polymorphs do not exceed 4.8 kcal·mol^{−1},^[47b] nonetheless, as discussed elsewhere,^[47c,d] up to 10 kcal·mol^{−1} energy differences among clusters leading to crystals with Ni, Pd, Pt, Rh and Ir are found. In particular, for their Rh containing clusters the differences are as large as 7.4 kcal·mol^{−1}. These numbers provide strong justification for our calculations. The fact that **4α** is more tightly bonded than **4β** helps explaining that the ball milling initially led to the formation of **4α**, which upon mechanical activation transforms into **4β**. Under equilibrium conditions the Ostwald's rule of stages states that crystallization follows a path from metastable to gradually more stable products. However, recently Frišćić and coworkers reported an exception to this rule in a mechanochemical system.^[48]

As shown in Figure 4b, the noncovalent interactions (NCI) descriptor using promolecular densities indicates that the stabilization in both **4α** and **4β** BHQ-[Cp*RhCl₂]₂ clusters is a consequence of an attractive fluxional wall of charge transferred from the molecular fragments to the interstitial region in both cases (the same fluxional walls are also observed in all the larger clusters (Figure S18–S19)). The relative strength of the attractive wall is directly tied to the size of the surface,^[46,49] which is larger for the clusters leading to **4α**. Quantitative evidence in favor of stronger interactions leading to a more stabilized **4α** cocrystal is obtained from the collective action of a larger number of intermolecular C–H...Cl and C–H...π contacts within each **4α** cluster as shown in Figure 2, as well as in the QTAIM plots (Figure 5a). Specifically, the 2Rc + 3BHQ **4α** cluster shows 6 C–H...Cl and 16 C–H...π contacts while the **4β** shows 4 C–H...Cl and 8 C–H...π (Figure 5). Gratifyingly, the intermolecular interactions found in the vertically grown clusters are also obtained in the extended solid QTAIM calculations, thus, our approach seems to rest on solid grounds. The lateral interactions in the extended solid are shown in the bonding paths coming out of the unit cell (Figure S20–S21).

Additionally, we obtained insight into the reactivity of both crystalline phases using the condensed dual Fukui indices,^[50–53] for nucleophilicity and electrophilicity (see Figure 5b) calculated at all atomic positions as $f^{(2)} = f^+ - f^-$ in the clusters. It is clear that in the 2Rc + 3BHQ clusters of **4α** one of the rhodium centers is an electrophile ($f^{(2)} = +0.026$) and the other one is a nucleophile ($f^{(2)} = -0.289$), it is also seen that two of the terminal chloride centers are nucleophiles ($f^{(2)} = -0.468, -0.033$) while one more is an electrophile ($f^{(2)} = +0.005$) and the remaining terminal chloride is not activated. Comparing the Fukui indices for **4α** to the ones for the isolated [Cp*RhCl₂]₂ (Figure S22), it is

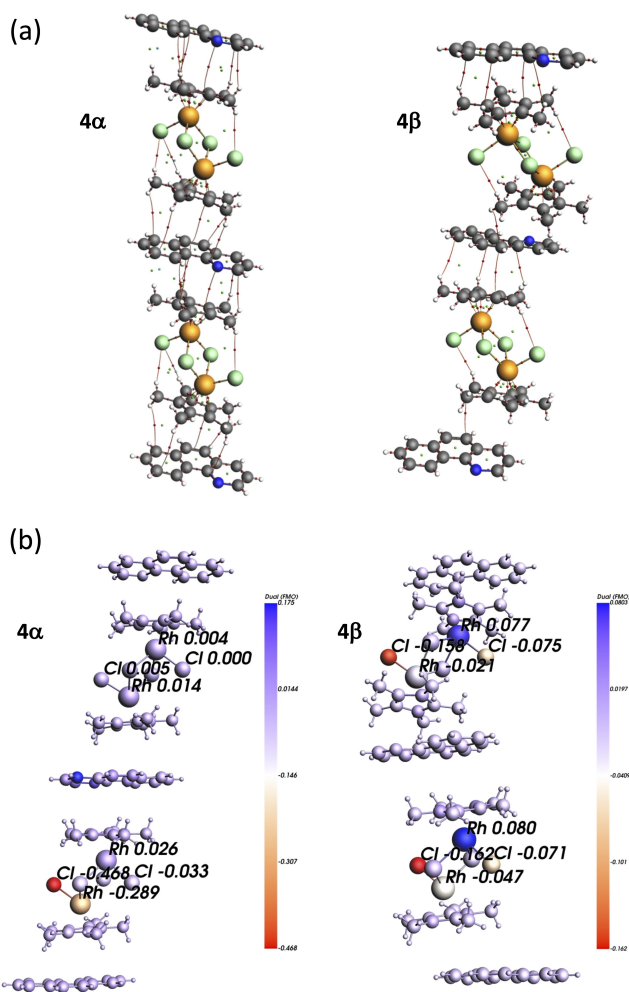


Figure 5. a) QTAIM plots for **4α** and **4β**. b) Molecular structures of **4α** and **4β** showing the condensed electrophilic and nucleophilic powers; nucleophilic parts are marked in red and electrophilic parts in blue.

evident that cocrystal **4α** is not well suited to undergo chemical reactions in which the rhodium centers act as electrophiles and the chloride centers act as nucleophiles. Conversely, in the **4β** cluster, there are two active electrophile rhodium centers ($\rho^{(2)} = +0.077$ and $+0.080$) and four active nucleophile terminal chloride centers ($\rho^{(2)} = -0.162, -0.158, -0.075, -0.071$). These numbers in conjunction with the above exposed fact that **4α** is more strongly bonded, help explaining why the $[\text{Cp}^*\text{RhCl}_2]_2$ units within **4β** are the more reactive species by far.

In-situ monitoring of the mechanochemical C–H bond activation

Experimentally, the cyclorhodation of the BHQ (**2**) requires that the $[\text{Cp}^*\text{RhCl}_2]_2$ units within the cocrystal react with NaOAc to generate species such as $[\text{Cp}^*\text{Rh}(k^2\text{-OAc})\text{Cl}]$.^[20–23,54] Therefore, being **4β** more activated than **4α** to undergo a double displacement reaction (metathesis reaction)^[55] with the base [Eq. (1)], **4β** should be more reactive to undertake the steps needed for the C–H activation of **2**.



In fact, our previous study found that the metalation of N–Heterocycles (e.g., BHQ (**2**), phenylpyridine, and 2-phenylquinoline) with $[\text{Cp}^*\text{MCl}_2]_2$ ($\text{M}=\text{Rh}, \text{Ir}$), and NaOAc would only start from **4β** or from isostructural or similar cocrystals.^[19] In the present work, the difference in reactivity between **4α** and **4β** in the presence of NaOAc was experimentally confirmed after carrying out the in-situ monitoring by synchrotron powder X-ray diffraction of the cyclorhodation of BHQ (**2**) with $[\text{Cp}^*\text{RhCl}_2]_2$ (**1**) and NaOAc (Figure S23). Such an experiment initially generated **4α**, which transformed into **4β** before diffraction features belonging to the corresponding rhodacycle **3** and NaCl could be detected. Compared to our previous study,^[19] the mechanochemical cyclorhodation of BHQ (**2**) at the synchrotron facilities proceeded at a slower pace producing small amounts of rhodacycle **3** after 2 h of milling at 30 Hz (Figure S23). This could have been due to the lower temperature inside the synchrotron experimental hutch (ca. 22 °C) in contrast to the warmer ambient temperature in the research laboratory.

Then, to facilitate the mechanochemical reaction of cocrystal **4β** with NaOAc, the experiment at the synchrotron was repeated this time by thermal ball milling^[39,56–60] (Figure 6) in a newly developed setup, which enabled XRD data collection while ball milling at high temperature (6d-f).^[61] Under these new reaction conditions (i.e., 40 °C), the diffraction signals of $[\text{Cp}^*\text{Rh}(\text{BHQ})\text{Cl}]$ **3** began appearing after only 7 min of milling and by the end of the 90-minute experiment rhodacycle **3** was the main product in the reaction mixture (Figure 6a–b), thus proving the involvement of **4β** as an intermediate in the reaction. Similarly, the progress of the C–H activation of BHQ could be monitored following the formation of NaCl (Figure 6c), which is generated after a chloride-to-acetate ligand exchange.^[62] The data therefore suggests that after the formation of the more activated cocrystal **4β**, the mechanochemical C–H cleavage involves chloride to acetate ligand substitution at the Rh^{III} center with the carboxylate acting as a ligand and as an intramolecular base. Probably NaOAc reacted with the rhodium atoms found close to the surface of the cocrystal **4β** particles, while further grinding could have exposed new unreacted surface of cocrystal **4β**. Importantly, under the in-situ monitoring conditions no other intermediates (e.g., $[\text{Cp}^*\text{Rh}(k^2\text{-OAc})\text{Cl}]$) were detected, which does not preclude their existence. This could be just a consequence of some intermediates being short-lived or perhaps non-crystalline, which would render them undetectable by the X-ray powder diffraction approach used in this study. However, this work clearly demonstrates the value of in-situ synchrotron X-ray powder diffraction monitoring to gain a better understanding of mechanochemical reactions such as C–H activations, which certainly complements the findings obtained with other monitoring techniques such as Raman spectroscopy.^[31–34]

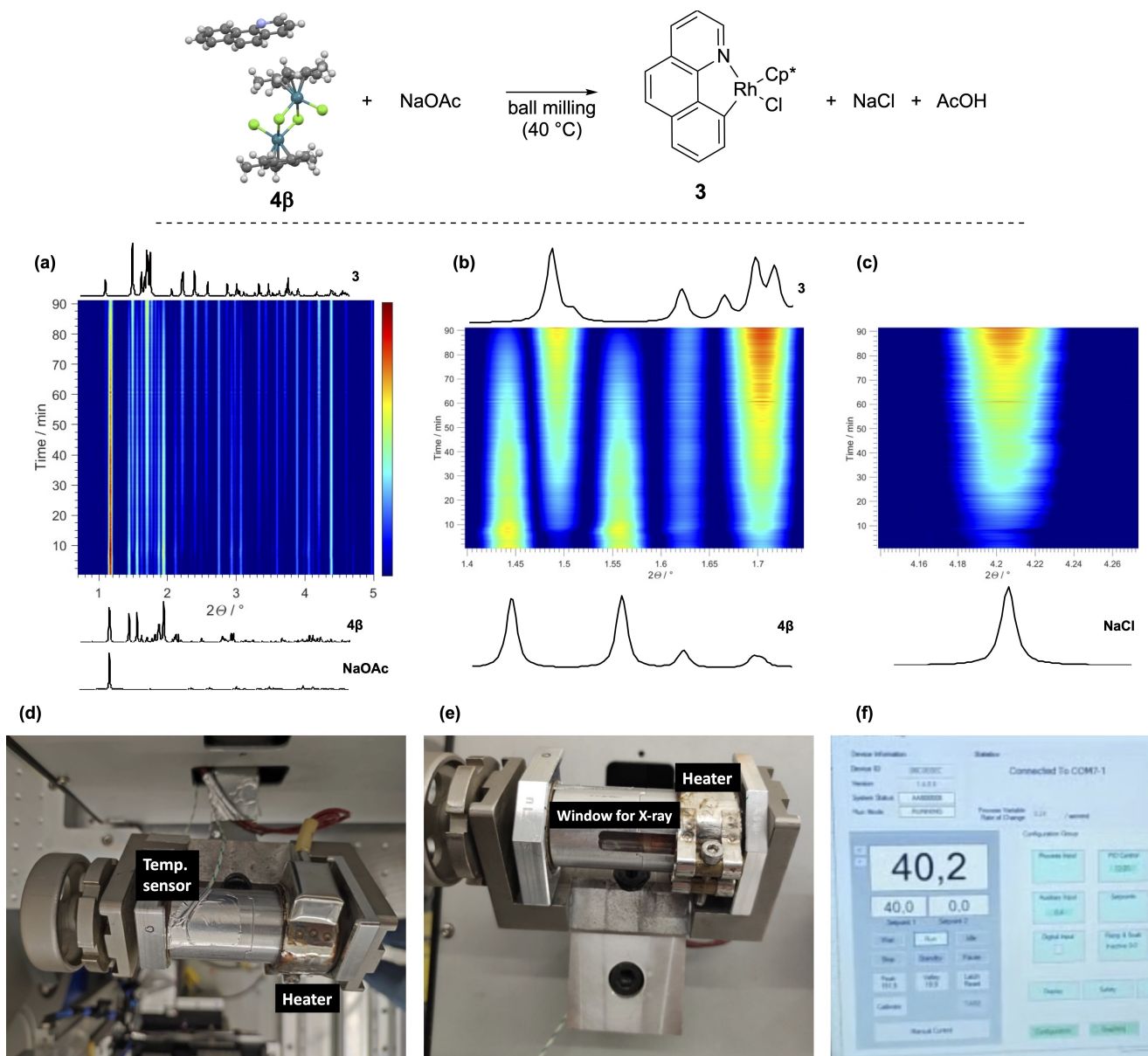


Figure 6. In-situ synchrotron X-ray powder diffraction monitoring of the mechanochemical reaction of cocrystal **4β** with NaOAc ($\lambda = 0.20741 \text{ \AA}$). a) Full time-resolved diffractograms for the reaction of **4β** (0.24 mmol) and NaOAc (6.0 equiv.) at 30 Hz and 40 °C. PXRD patterns of **4β**, NaOAc, and **3** are given on the bottom and at the top of the 2D plot. Crystallographic data used in the PXRD analysis: **3** (CCDC code: ROJCUP). b) Expansion of time-resolved diffractograms evidencing the formation of rhodacycle **3**. c) Expansion of time-resolved diffractograms showing the concomitant formation of NaCl during the cyclorhodation of BHQ (**2**). d)–e) Photographs (top and front view) of the milling jar and set up used for in-situ monitoring of the reaction by synchrotron X-ray powder diffraction. f) Photograph of the temperature recording during the thermal milling.

Conclusions

In this study, we implemented for the first time in-situ synchrotron X-ray powder diffraction to monitor a mechanochemical cyclorhodation reaction in a ball mill. Specifically, we investigated the reaction of benzo[*h*]quinoline with $[\text{Cp}^*\text{RhCl}_2]_2$ and found that two crystalline reaction intermediates appeared between the reagents during the ball milling process before the C–H activation step. Additionally, in-situ analysis of the reaction enabled us to observe the mechanochemical polymorphic transformation of the early-appearing cocrystal **4α** into its polymorph **4β**. Importantly, analysis by in-situ variable-temper-

ature powder X-ray diffraction demonstrated that the mechanochemical solid-state polymorphic transformation is promoted at temperatures lower than those required by heating alone. Moreover, experimental and computational analysis enabled us to identify the origin of the stability in **4α** and **4β** as well as revealing their structural and electronic differences. Computationally we found that differences in the crystal packing between both cocrystals and disparities in their intermolecular interactions make the $[\text{Cp}^*\text{RhCl}_2]_2$ units in **4β** more activated towards the reaction with NaOAc than in cocrystal **4α**. This was corroborated experimentally during in-situ monitoring of the mechanochemical C–H bond cleavage of BHQ with $[\text{Cp}^*\text{RhCl}_2]_2$

and NaOAc and from the reaction of **4β** with NaOAc, which led to the formation of the rhodacycle [Cp*Rh-(BHQ)Cl] **3**.

Until now, the beneficial role of crystalline intermediates in mechanochemical reactions had mainly been related to the regular arrangement of the reagents gained within the cocrystals, which can position the reaction partners in proximity for the reactions to proceed. However, this study demonstrates that mechanochemistry can also provide the conditions for noncovalent interactions to arise, and guide chemical transformations through the formation of crystalline supramolecular assemblies that can affect the electrophilicity and nucleophilicity of the reactive centers. And as the formation and persistence of such weak interactions might be absent in solution, this could help explain why some substrates that failed or only gave traces of the corresponding rhodacycles in solution,^[24,63,64] have been reported to undergo cyclorhodation by mechanochemistry.^[19,24]

Experimental Section

Chemicals: Benzo[*h*]quinoline (>99% purity, TCI) and NaOAc (>99% purity, Kemika) were used as received from the commercial supplier. [Cp*RhCl₂]₂ was synthesized according to the literature.^[65,66]

Milling equipment: Mechanochemical reactions were carried out using an IST-636 mixer mill (InSolido Technologies, Zagreb, Croatia) at 30 Hz using milling jars made of poly(methyl) methacrylate (PMMA; 15 mL in internal volume) and one milling ball made of ZrO₂ weighing 3.4 g.

Powder X-ray diffraction: PXRD patterns were collected on a PanAnalytical Aeris diffractometer (Cu_{Kα} radiation and Ni filter) in Bragg–Brentano geometry using a zero-background sample holder.

Deposition Numbers CLCPRH (for **1**), XAWPUK (for **4α**), and XAWPUK01 (for **4β**) contain the supplementary crystallographic data for this paper. These data are provided free of charge by the joint Cambridge Crystallographic Data Centre and Fachinformationszentrum Karlsruhe Access Structures service.

In-situ variable-temperature powder X-ray diffraction: VT-PXRD data were collected using a Malvern Panalytical Empyrean powder diffractometer (Malvern Panalytical B.V., Almelo, The Netherlands) in the Debye–Scherrer geometry with a PIXcel1D detector equipped with dCore automatic diffracted beam optics, using Cu_{Kα} radiation (λ = 1.5406 Å) and focusing W/Si elliptical mirror and transmission anti-scatter device on the incident beam side. Samples were contained in a transmission cell (0.2 mm sample thickness) as a part of Anton Paar TTK 600 variable temperature sample environment. Diffraction intensities were collected isothermally (30 min collection time) in temperature range of 30–300 °C every 10 °C and in range of 5–40° 2θ, in continuous mode with step size of 0.0131° 2θ and collection time of 39.6 s per point.

In-situ monitoring of the mechanochemical reactions by synchrotron X-ray diffraction: Synchrotron X-ray diffraction monitoring was performed at P02.1 beamline at PETRA III, Deutsches Elektronen-Synchrotron (DESY) using X-rays of λ = 0.20741 Å and a Perkin Elmer XRD 1621 flat panel detector consisting of an amorphous Si sensor equipped with a CsI scintillator (pixel number 2048 × 2048, pixel size 200 × 200 μm²). Data processing was accomplished following protocols reported before.^[27] Patterns were collected with time resolution of 5 s. 2D time-resolved plots of in-

situ monitoring data were created in MATLAB and the background of each diffraction pattern was subtracted prior to plotting using the Sonneveld-Visser algorithm.^[67]

Thermogravimetric analysis: TGA was carried out with a Mettler-Toledo TGA/DSC 3+ thermobalance (Mettler Toledo, Columbus, OH, USA) using alumina crucibles (70 μL). Between 5.0 mg and 7.0 mg of sample were used. All experiments were recorded in a dynamic nitrogen atmosphere with a flow rate of 50 cm³·min⁻¹ and with heating rate of 10 K·min⁻¹.

Differential scanning calorimetry analysis: The analysis was performed with a TA DSC 25 calorimeter using standard aluminum pans. Between 1.0 and 2.0 mg of sample were used. All experiments were conducted in a dynamic nitrogen atmosphere with a flow rate of 50 cm³ min⁻¹ and with heating rate of 10 K·min⁻¹.

Mechanochemical cocrystal formation: A mixture of [Cp*RhCl₂]₂ (**1**, 150 mg, 0.242 mmol) and BHQ (0.484 mmol) was milled in a 15 mL PMMA milling vessel with one ZrO₂ milling ball weighing 3.4 g in a mixer mill at 30 Hz.

Mechanochemical cyclorhodation without external heating: A mixture of [Cp*RhCl₂]₂ (**1**, 150 mg, 0.242 mmol), BHQ (0.484 mmol) and sodium acetate (120 mg, 1.463 mmol) was milled in a 15 mL PMMA milling vessel with one ZrO₂ milling ball weighing 3.4 g in a mixer mill at 30 Hz.

Mechanochemical cyclorhodation at high temperature: Monitoring of the mechanochemical cyclorhodation reaction at 40 °C by synchrotron X-ray diffraction was carried out as described above using a newly developed setup, which enabled XRD data collection while ball milling at high temperature (Figure 6). For this, **4β** (237 mg) and sodium acetate (120 mg, 1.463 mmol) were milled in a 15 mL PMMA milling vessel with one ZrO₂ milling ball weighing 3.4 g in a mixer mill at 30 Hz.

Supporting Information

Detailed experimental, analytical, and computational data are contained in the Supporting Information.

Acknowledgements

J.G.H and K.J.A.F acknowledge the internal support from Universidad de Antioquia through the project CODI 2022-48630. This work was supported in part by the “Research Cooperability” Program of the Croatian Science Foundation funded by the European Union from the European Social Fund under the Operational Programme Efficient Human Resources 2014–2020, through grant PZS-2019-02-4129. T.S. acknowledges the Croatian Science Foundation (grant no. IP-2020-02-4702) for financial support and DESY (Hamburg, Germany), a member of the Helmholtz Association HGF, for the provision of experimental facilities. Parts of this research were carried out at PETRA III and T.S. thanks Dr. Martin Etter for assistance in using beamline P02.1. Beamtime was allocated for proposal I-20220019 EC. M.R. and E.T. acknowledge the support of project CluK co-financed by the Croatian Government and the European Union through the European Regional Development Fund-Competitiveness and Cohesion Operational Programme (grant KK.01.1.1.02.0016).

Conflict of Interests

The authors declare no conflict of interest.

Data Availability Statement

The data that support the findings of this study are available in the supplementary material of this article.

Keywords: ball milling · C–H activation · cyclorhodation · in situ monitoring · mechanochemistry

- [1] K. J. Ardila-Fierro, J. G. Hernández, *ChemSusChem* **2021**, *14*, 2145–2162.
- [2] N. Fantozzi, J.-N. Volle, A. Porcheddu, D. Virieux, F. García, E. Colacino, *ChemRxiv*, preprint, DOI: 10.26434/chemrxiv-2022-b370p, **2022**.
- [3] J.-L. Do, T. Friščić, *ACS Cent. Sci.* **2017**, *3*, 13–19.
- [4] J. G. Hernández, C. Bolm, *J. Org. Chem.* **2017**, *82*, 4007–4019.
- [5] F. Cuccu, L. De Luca, F. Delogu, E. Colacino, N. Solin, R. Mocchi, A. Porcheddu, *ChemSusChem* **2022**, *15*, e202200362.
- [6] T. Friščić, S. L. Childs, S. A. A. Rizvi, W. Jones, *CrystEngComm* **2009**, *11*, 418–426.
- [7] N. Shan, F. Toda, W. Jones, *Chem. Commun.* **2002**, 2372–2373.
- [8] P. A. Julien, I. Malvestiti, T. Friščić, *Beilstein J. Org. Chem.* **2017**, *13*, 2160–2168.
- [9] A. M. Belenguer, A. A. L. Michalchuk, G. I. Lampronti, J. K. M. Sanders, *Beilstein J. Org. Chem.* **2019**, *15*, 1226–1235.
- [10] E. Machuca, E. Juaristi, *Tetrahedron Lett.* **2015**, *56*, 1144–1148.
- [11] J. L. Howard, Y. Sagatov, L. Repusseau, C. Schotten, D. L. Browne, *Green Chem.* **2017**, *19*, 2798–2802.
- [12] J. L. Howard, M. C. Brand, D. L. Browne, *Angew. Chem. Int. Ed.* **2018**, *57*, 16104–16108.
- [13] M. Arhangelskis, D.-K. Bučar, S. Bordignon, M. R. Chierotti, S. A. Stratford, D. Voinovich, W. Jones, D. Hasa, *Chem. Sci.* **2021**, *12*, 3264–3269.
- [14] R. F. Koby, T. P. Hanusa, N. D. Schley, *J. Am. Chem. Soc.* **2018**, *140*, 15934–15942.
- [15] a) S. Lukin, M. Tireli, I. Lončarić, D. Barišić, P. Šket, D. Vrsaljko, M. di Michiel, J. Plavec, K. Užarević, I. Halasz, *Chem. Commun.* **2018**, *54*, 13216–13216; b) M. Kralj, S. Lukin, G. Miletić, I. Halasz, *J. Org. Chem.* **2021**, *86*, 14160–14168.
- [16] T. Stolar, K. Užarević, *CrystEngComm* **2020**, *22*, 4511–4525.
- [17] Z. Akimbekov, A. D. Katsenis, G. P. Nagabhushana, G. Ayoub, M. Arhangelskis, A. J. Morris, T. Friščić, A. Navrotsky, *J. Am. Chem. Soc.* **2017**, *139*, 7952–7957.
- [18] a) A. N. Sokolov, D.-K. Bučar, J. Baltrusaitis, S. X. Gu, L. R. MacGillivray, *Angew. Chem. Int. Ed.* **2010**, *49*, 4273–4277; b) J. Stojaković, B. S. Farris, L. R. MacGillivray, *Faraday Discuss.* **2014**, *170*, 35–40; c) E. Elacqua, K. A. Kummer, R. H. Groeneman, E. W. Reinheimer, L. R. MacGillivray, *J. Photochem. Photobiol. A.* **2016**, *331*, 42–47.
- [19] K. J. Ardila-Fierro, M. Rubčić, J. G. Hernández, *Chem. Eur. J.* **2022**, *28*, e202200737.
- [20] D. L. Davies, O. Al-Duaij, J. Fawcett, M. Giardiello, S. T. Hilton, D. R. Russell, *Dalton Trans.* **2003**, 4132–4138.
- [21] L. Li, W. W. Brennessel, W. D. Jones, *J. Am. Chem. Soc.* **2008**, *130*, 12414–12419.
- [22] Y. Boutadla, O. Al-Duaij, D. L. Davies, G. A. Griffith, K. Singh, *Organometallics* **2009**, *28*, 433–440.
- [23] A. I. Vander Weide, W. W. Brennessel, W. D. Jones, *J. Org. Chem.* **2019**, *84*, 12960–12965.
- [24] S. Ni, M. Hribersek, S. K. Baddigam, F. J. L. Ingner, A. Orthaber, P. J. Gates, L. T. Pilarski, *Angew. Chem. Int. Ed.* **2021**, *60*, 6660–6666.
- [25] P. A. Julien, T. Friščić, *Cryst. Growth Des.* **2022**, *22*, 5726–5754.
- [26] A. A. L. Michalchuk, F. Emmerling, *Angew. Chem. Int. Ed.* **2022**, *61*, e202117270.
- [27] I. Halasz, S. A. J. Kimber, P. J. Beldon, A. M. Belenguer, F. Adams, V. Honkimäki, R. C. Nightingale, R. E. Dinnebier, T. Friščić, *Nat. Protoc.* **2013**, *8*, 1718–1729.
- [28] K. Užarević, I. Halasz, T. Friščić, *J. Phys. Chem. Lett.* **2015**, *6*, 4129–4140.
- [29] S. Lukin, L. S. Germann, T. Friščić, I. Halasz, *Acc. Chem. Res.* **2022**, *55*, 1262–1277.
- [30] A. A. L. Michalchuk, A. Kabelitz, F. Emmerling in *Nontraditional Activation Methods in Green and Sustainable Applications* (Eds.: B. Török, C. Schäfer), Elsevier, **2021**, pp 369–419.
- [31] M. Juribašić, K. Užarević, D. Gracin, M. Čurić, *Chem. Commun.* **2014**, *50*, 10287–10290.
- [32] A. Bjelopetrović, Lukin, S. I. Halasz, K. Užarević, K. Dilović, D. Barišić, A. Budimir, M. Juribašić-Kulcsár, M. Čurić, *Chem. Eur. J.* **2018**, *24*, 10672–10682.
- [33] D. Barišić, I. Halasz, A. Bjelopetrović, D. Babić, M. Čurić, *Organometallics* **2022**, *41*, 1284–1294.
- [34] D. Barišić, M. Pajić, I. Halasz, D. Babić, M. Čurić, *Beilstein J. Org. Chem.* **2022**, *18*, 680–687.
- [35] D. P. Malenov, J. P. Blagojević Filipović, S. D. Zarić, *Acta Crystallogr. Sect. B Struct. Sci. Cryst. Eng. Mater.* **2020**, *76*, 252–258.
- [36] T. Friščić, R. W. Lancaster, L. Fábrián, P. G. Karamertzanis, *Proc. Natl. Acad. Sci. USA* **2010**, *107*, 13216–13221.
- [37] K. J. Ardila-Fierro, V. André, D. Tan, M. T. Duarte, R. W. Lancaster, P. G. Karamertzanis, T. Friščić, *Cryst. Growth Des.* **2015**, *15*, 1492–1501.
- [38] K. J. Ardila-Fierro, S. Lukin, M. Etter, K. Užarević, I. Halasz, C. Bolm, J. G. Hernández, *Angew. Chem. Int. Ed.* **2020**, *59*, 13458–13462.
- [39] K. Linberg, B. Röder, D. Ai-Sabbagh, F. Emmerling, A. A. L. Michalchuk, *Faraday Discuss.* **2023**, *241*, 178–193.
- [40] a) R. Marc, R. Tonner, *J. Chem. Phys.* **2015**, *142*, 194105; b) S. Grimme, C. Bannwarth, P. Shushkov, *J. Chem. Theory Comput.* **2017**, *13*, 1989–2009.
- [41] a) J. P. Perdew, K. Burke, M. Ernzerhof, *Phys. Rev. Lett.* **1996**, *77*, 3865–3868; b) J. P. Perdew, K. Burke, M. Ernzerhof, *Phys. Rev. Lett.* **1997**, *78*, 1396; c) S. Grimme, J. Antony, S. Ehrlich, H. Krieg, *J. Chem. Phys.* **2010**, *132*, 144104.
- [42] R. Rüger, M. Franchini, T. Trnka, A. Yakovlev, E. van Lenthe, P. Philipsen, T. van Vuren, B. Klumpers, T. Soini, *AMS 2022.1, SCM, Theoretical Chemistry, Vrije Universiteit, Amsterdam, The Netherlands*, <http://www.scm.com>.
- [43] G. te Velde, E. J. Baerends, *Phys. Rev. B.* **1991**, *44*, 7888.
- [44] P. H. T. Philipsen, G. te Velde, E. J. Baerends, J. A. Berger, P. L. de Boeij, M. Franchini, J. A. Groeneveld, E. S. Kadantsev, R. Klooster, F. Kootstra, M. C. W. M. Pols, P. Romaniello, M. Raupach, D. G. Skachkov, J. G. Snijders, C. J. O. Verzijl, J. A. Celis Gil, J. M. Thijssen, G. Wiesenecker, C. A. Peebles, G. Schreckenbach, T. Ziegler, *BAND 2022.1, SCM, Theoretical Chemistry, Vrije Universiteit, Amsterdam, The Netherlands*, <http://www.scm.com>.
- [45] J. I. Rodríguez, *J. Comput. Chem.* **2012**, *34*, 681–688.
- [46] a) E. R. Johnson, S. Keinan, P. Mori-Sánchez, J. Contreras-García, A. J. Cohen, W. Yang, *J. Am. Chem. Soc.* **2010**, *132*, 6498–6506; b) J. Contreras-García, E. R. Johnson, S. Keinan, R. Chaudret, J.-P. Piquemal, D. N. Beratan, W. Yang, *J. Chem. Theory Comput.* **2011**, *7*, 625–632.
- [47] a) S. F. Boys, F. J. M. P. Bernardi, *Mol. Phys.* **1970**, *19*, 553–566; b) J. Nyman, G. M. Day, *CrystEngComm* **2015**, *17*, 5154–5165; c) G. Aullón, G. Ujaque, A. Lledós, S. Alvarez, P. Alemany, *Inorg. Chem.* **1998**, *37*, 804–813; d) D. R. Ullery, C. E. Moore, C. M. Thomas, *Acta Crystallogr. Sect. E Crystallogr. Commun.* **2021**, *77*, 871–874.
- [48] L. S. Germann, M. Arhangelskis, M. Etter, R. E. Dinnebier, T. Friščić, *Chem. Sci.* **2020**, *11*, 10092–10100.
- [49] A. Otero-de-la-Roza, E. R. Johnson, J. Contreras-García, *Phys. Chem. Chem. Phys.* **2012**, *14*, 12165–12172.
- [50] H. Chermette, *J. Comput. Chem.* **1999**, *20*, 129–154.
- [51] P. Geerlings, F. De Proft, W. Langenecker, *Chem. Rev.* **2003**, *103*, 1793–1874.
- [52] C. Morell, A. Grand, A. Toro-Labbé, *J. Phys. Chem. A.* **2005**, *109*, 205–212.
- [53] G. Hoffmann, V. Tognetti, L. Joubert, *J. Mol. Model.* **2018**, *24*, 281.
- [54] J. Li, W. Hu, Y. Peng, Y. Zhang, J. Li, W. Zheng, *Organometallics* **2014**, *33*, 2150–2159.
- [55] T. Auvray, T. Friščić, *Molecules* **2023**, *28*, 897.
- [56] V. Martínez, T. Stolar, B. Karadeniz, I. Brekalo, K. Užarević, *Nat. Chem. Rev.* **2023**, *7*, 51–65.
- [57] N. Cindro, M. Tireli, B. Karadeniz, T. Mrla, K. Užarević, *ACS Sustainable Chem. Eng.* **2019**, *7*, 16301–16309.
- [58] R. R. A. Bolt, S. E. Raby-Buck, K. Ingram, J. A. Leitch, D. L. Browne, *Angew. Chem. Int. Ed.* **2022**, *61*, e202210508.
- [59] J. Andersen, H. Starbuck, T. Current, S. Martin, J. Mack, *Green Chem.* **2021**, *23*, 8501–8509.
- [60] R. Takahashi, A. Hu, P. Gao, Y. Gao, Y. Pang, T. Seo, J. Jian, S. Maeda, H. Takaya, K. Kubota, H. Ito, *Nat. Commun.* **2021**, *12*, 6691.
- [61] N. Jakupec, K. J. Ardila-Fierro, V. Martínez, I. Halasz, J. Volavšek, G. Algara-Siller, M. Etter, V. Valtchev, K. Užarević, Ana Palčić, unpublished results.

- [62] The concomitantly formation of AcOH is noticeable by smell and can be confirmed by ^1H NMR spectroscopy.
- [63] X. Chu, S. Zhang, Z. Wang, T. Li, B. Zhu, *RSC Adv.* **2018**, *8*, 7164–7172.
- [64] L. Li, W. W. Brennessel, W. D. Jones, *Organometallics* **2009**, *28*, 3492–3500.
- [65] C. white, A. Yates, P. M. Maitlis, *Inorg. Synth.* **1992**, *29*, 228–3242.
- [66] J. G. Hernández, C. Bolm, *Chem. Commun.* **2015**, *51*, 12582–12584.
- [67] E. J. Sonneveld, J. W. Visser, *J. Appl. Crystallogr.* **1975**, *8*, 1–7.

Manuscript received: April 24, 2023
Accepted manuscript online: June 22, 2023
Version of record online: August 16, 2023